Magnetic helicity transport in the quiet Sun
by Brian Thomas Welsch

A dissertation submitted in partial fulfillment of the requirements for the degree of Doctor of Philosophy in Physics
Montana State University
© Copyright by Brian Thomas Welsch (2002)

Abstract:
The flux of magnetic helicity through the solar photosphere has implications in diverse areas of current solar research, including solar dynamo modelling and coronal heating. Other researchers have considered the flux of magnetic helicity from active regions; here, we do the same for quiet-sun magnetic fields. We derive a theoretical expression for the helicity flux in terms of the relative motions of separate flux elements, and the time evolution of the quadrupole moments of individual magnetic flux elements, summing both "mutual" and "self-helicity" contributions to get the total helicity flux. Using a tracking algorithm applied to high cadence, high resolution SOHO/MDI magnetograms, we determine the observed rate of helicity flux in the quiet sun and compare these measurements with our theoretical predictions.

MAGNETIC HELICITY TRANSPORT IN THE QUIET SUN

by

Brian Thomas Welsch

A dissertation submitted in partial fulfillment
of the requirements for the degree

of

Doctor of Philosophy

in

Physics

MONTANA STATE UNIVERSITY — BOZEMAN
Bozeman, Montana

February 2002

D378
W4639

APPROVAL

of a dissertation submitted by

Brian Thomas Welsch

This dissertation has been read by each member of the dissertation committee, and has been found to be satisfactory regarding content, English usage, format, citations, bibliographic style and consistency, and is ready for submission to the College of Graduate Studies.

Dana W. Longcope, Ph. D. _____ 2/21/02
(Signature) Date

Approved for the Department of Physics

John C. Hermanson, Ph. D. _____ 2-21-02
(Signature) Date

Approved for the College of Graduate Studies

Bruce R. McLeod, Ph. D _____ 2-22-02
(Signature) Date

STATEMENT OF PERMISSION TO USE

In presenting this dissertation in partial fulfillment of the requirements for a doctoral degree at Montana State University — Bozeman, I agree that the Library shall make it available to borrowers under rules of the Library. I further agree that copying of this thesis is allowable only for scholarly purposes, consistent with "fair use" as prescribed in the U. S. Copyright Law. Requests for extensive copying or reproduction of this thesis should be referred to University Microfilms International, 300 North Zeeb Road, Ann Arbor, Michigan, 48106, to whom I have granted "the exclusive right to reproduce and distribute my dissertation in and from microform along with the non-exclusive right to reproduce and distribute my abstract in any format in whole or in part."

Signature BRIAN WELSCH

Date 2/22/2

ACKNOWLEDGEMENTS

Giving thanks is a tricky business: I want to favor some who went out of their way to help me with a special mention, but I risk offending others by omission. If you feel that I have not properly recognized your contribution to my work in this acknowledgement, please accept my apology, know that I meant no disrespect, and forgive my imperfections! That said, I would like to thank: Dr. Loren Acton, for starting the solar physics group at Montana State – a lot of extra work he did not have to do; Dr. Dick Canfield, for always finding time to talk physics with me, though I knew him to be exceedingly busy; Dr. Dana Longcope, who taught me all the physics my tiny brain could take on board, and did so with both patience and a sense of humor; collectively, Margaret Jarrett, Jeannie Gunderson, and Rose Waldon, whose hard work allowed me to think about physics and not bureaucracy; my fellow graduate students, whose friendship and inspiration will remain in my mind always; and the other members of the University community who in countless small ways made my time here at Montana State an enjoyable one. Finally, I wish to thank those responsible for funding this work: the National Science Foundation (under grant ATM-9733424), the National Aeronautics and Space Administration (under grant NAG5-6110), and, primarily, the American taxpayer.

TABLE OF CONTENTS

1. INTRODUCTION 1

Manifestations of Magnetic Fields in the Solar Photosphere 1
What is Magnetic Helicity? 5
Why Study the Transport of Magnetic Helicity? 8
Current Research in Solar Magnetic Helicity Transport 12
The Present Contribution to the Study of Solar Magnetic Helicity Transport 13

2. THEORY OF HELICITY TRANSPORT 16

Relative Helicity, and Its Flux 16
Flux of Magnetic Helicity via Advection 18
Flux of Magnetic Helicity via Braiding 19
Theory of "Mutual Helicity" Transport 22
Applicability to the Sun 25
Theory of "Self Helicity" Transport 27
Applicability to the Sun 36
Example: A Rotating Bipole 42

3. METHODS 49

Data 49
Labelling 58
Tracking Algorithm 69
Finding the Mutual Helicity Flux 82
Finding the Self Helicity Flux 84
Flux Evolution & Measurable Flow Properties 85
Singular Value Decomposition 93
Relaxation Algorithm 95
Self Helicity Test 98

Application to Data 102

4. Predicted Quiet-Sun Helicity Flux 113

Expected Mutual Helicity Flux in MDI Hi-Res FOV 113
Average Relative Rotation Rate 117
Expected Self Helicity Flux in MDI FOV 119

5. Results 126

Mutual Helicity 126
Contributions to Helicity Flux 134
Integral Mutual Helicity Flux 139
Self Helicity 141
Spatial Distribution of Self-Helicity Flux 147
Comparison of Mutual and Self Helicity Fluxes 154
Archived Results 155

6. Discussion 157

Summary 157
Additional Results 159
Implications of Our Results 161
Conclusion 162

APPENDICES 164
A. Kinetic Helicity & Energy in Photospheric Flows 165
B. Expected Mutual Helicity Flux in MDI FOV 170
C. Error Analysis 182

BIBLIOGRAPHY 198

LIST OF TABLES

Table		Page
3.1	Summary of Data Sets' Properties	55
3.2	Flux Elements' Properties	63
3.3	Elements' Characteristic Values	67
3.4	Properties of Flux Elements' Shape-Distributions	69
5.1	Mutual Helicity Fluxes	128
5.2	Self Helicity Fluxes	145
B.1	Data Sets' Expected Average Relative Rotation Rate	180
C.1	Shape-Finding Routine Test Results	188
C.2	Mutual Helicity Flux Routine Test Results	193

LIST OF FIGURES

Figure		Page
1.1	Two Linked Flux Tubes	7
2.1	Quiet Sun Magnetic Fields Exist in Isolated Regions	20
2.2	Circumferential Vector Potential	24
2.3	Sign of Mutual Helicity Flux	25
2.4	Differential Rotation Braids Footpoints	26
2.5	Coordinates from Center of Flux	28
2.6	Flux Shapes	32
2.7	Elementary Flow Patterns	35
2.8	Flux Distributions Combined With Flows "Generate" Helicity	36
2.9	Supergranulation Pattern in MDI Data	39
2.10	Coriolis-Induced Vorticity in Turbulence Spins Fluxes	41
2.11	Coordinate System in Rotating Bipole Example	43
2.12	"Rigid Rotation" and "Constant Orientation" Assumptions	47
3.1	MDI Hi-Res FOV	51

3.2 Images from Data Sets # 1 and 2a 52

3.3 Images from Data Sets # 2b and 2c 53

3.4 Image from Data Set # 3 53

3.5 Histograms of Pixels' Field Strengths. 56

3.6 Histograms of Flux Element Properties in Data Set # 1 63

3.7 Histograms of Flux Element Properties in Data Set # 2a 64

3.8 Histograms of Flux Element Properties in Data Set # 2b 64

3.9 Histograms of Flux Element Properties in Data Set # 2c 65

3.10 Histograms of Flux Element Properties in Data Set # 3 65

3.11 Histograms of Shape Coefficients in Data Set # 1 67

3.12 Example Flux Element: F_0 Mode 70

3.13 Example Flux Element: F_2 Mode 70

3.14 Example Flux Element: G_2 Mode. 71

3.15 Submergence, Emergence, and One-to-One Matching of Fluxes . . . 73

3.16 Colliding Flux Elements 75

3.17 Tracked Velocities in Set # 1 77

3.18 Tracked Velocities in Set # 2a 78

3.19 Tracked Velocities in Set # 2b 79

3.20 Tracked Velocities in Set # 2c 80

3.21 Tracked Velocities in Set # 3 81

3.22 Geometry of Relative Rotation 84

3.23 Flows in Null Space of Shape Matrix 93

3.24 Test Iversion: Data 99

3.25 Test Iversion: Graphs 100

3.26 Test Iversion: Surface Plots 101

3.27 Iversion of Data: Graphs. 103

3.28 Inversion of Data, Surfaces 104

3.29 Spikes & Flux Element Disruptions 106

3.30 Relaxation of Subintervals 109

3.31 Relaxation with Left & Right Endpoints Fixed 111

3.32 Relaxation with Neither & Both Endpoints Fixed 112

5.1 Mutual Helicity Flux in Set # 1 129

5.2 Mutual Helicity Flux in Set # 2a 129

5.3 Mutual Helicity Flux in Set # 2b 130

5.4 Mutual Helicity Flux in Set # 2c 130

5.5 Mutual Helicity Flux in Full Set # 3 131

5.6 Mutual Helicity Flux in Truncated Set # 3 131

5.7 Magnetogram Late in Tracking Run # 3 132

5.8 Final Image from Truncated Data Set # 3 132

5.9 Contributions to Helicity Flux in Set # 1 136

5.10 Contributions to Helicity Flux in Set # 2a 137

5.11 Contributions to Helicity Flux in Set # 2b 137

5.12 Contributions to Helicity Flux in Set # 2c 138

5.13 Contributions to Helicity Flux in Set # 3 138

5.14 Steps Tracked as a Function of Flux 143

5.15 Elements Tracked as a Function of Tracking Duration 145

5.16 $d\mathcal{H}^{(\mathrm{SELF})}/dt$ Examples 146

5.17 Self Helicity Flux in Set # 1 147

5.18 Self Helicity Flux in Set # 2a 148

5.19 Self Helicity Flux in Set # 2b 148

5.20 Self Helicity Flux in Set # 2c 149

5.21 Self Helicity Flux in Set # 3 149

5.22 $d\mathcal{H}^{(\mathrm{SELF})}/dt$ vs. Latitude, in Data Set # 1 150

5.23 $d\mathcal{H}^{(\mathrm{SELF})}/dt$ vs. Latitude, in Data Set # 2a 150

5.24 $d\mathcal{H}^{(\mathrm{SELF})}/dt$ vs. Latitude, in Data Set # 2b 151

5.25 $d\mathcal{H}^{(\mathrm{SELF})}/dt$ vs. Latitude, in Data Set # 2c 151

5.26 $d\mathcal{H}^{(\mathrm{SELF})}/dt$ vs. Latitude, in Data Set # 3 152

5.27 Scatter Plots of Self-Helicity Flux From Set # 1 153

A.1 Comparison of Scaled Kinetic Helicity & Kinetic Energy 168

C.1 Tests of Mutual Helicity Finder 193

ABSTRACT

The flux of magnetic helicity through the solar photosphere has implications in diverse areas of current solar research, including solar dynamo modelling and coronal heating. Other researchers have considered the flux of magnetic helicity from active regions; here, we do the same for quiet-sun magnetic fields. We derive a theoretical expression for the helicity flux in terms of the relative motions of separate flux elements, and the time evolution of the quadrupole moments of individual magnetic flux elements, summing both "mutual" and "self-helicity" contributions to get the total helicity flux. Using a tracking algorithm applied to high cadence, high resolution SOHO/MDI magnetograms, we determine the observed rate of helicity flux in the quiet sun and compare these measurements with our theoretical predictions.

CHAPTER 1

INTRODUCTION

'If it were not for its variable magnetic field, the Sun would have been a rather uninteresting star.' – E.N. Parker

Manifestations of Magnetic Fields in the Solar Photosphere

Observations of the Sun's visible surface, the photosphere, demonstrate the presence of magnetic fields over a range of spatial scales. The magnetic fields composing this continuous spectrum are usually lumped into two categories: "active region" fields, near the large end of the spectrum, and "quiet sun" fields, near the small end.

Both populations are thought to be composed of sub-resolution magnetic flux tubes, each with a typical magnetic field strength (or magnetic flux density) $|\mathbf{B}|$ on the order of 10^3 Gauss (Stenflo 1994), but the density (or "filling factor") of flux tubes in quiet-sun fields is much lower than in active-region fields. Consequently, average field strengths in quiet-sun fields at resolutions currently attainable are much lower than average field strengths in active region fields.

In addition to differences in average field strengths, comparisons of their typical sizes, spatial distributions, and temporal evolution highlight the differences between the two populations.

Concentrated active-region fields typically extend for tens of megameters (Mm) or more. These features are commonly referred to as sunspot fields, or sunspots. Typical active region fields often contain more that $\sim 10^{21}$ maxwells (1 Mx = 1 Gauss $\cdot$cm^2) of unsigned magnetic flux, with average magnetic field strengths of the order of 1 kG. Because the presence of strong magnetic fields over a large area can noticeably affect the appearance of the Sun's visible surface, active-region fields are the oldest known manifestation of magnetism on the Sun: records of sunspot observations by Chinese observers exist as far back as A.D. 301.

Active-region fields are not always present in the photosphere, and they are not distributed uniformly over the surface at any time. The presence of active region fields oscillates with an 11-year period, known as the solar cycle, and active regions are observed only within about 35° heliocentric latitude of the Sun's equator. Bipolar active region fields have been observed "emerging" through the photosphere, beginning at relatively high latitudes near "solar minimum," when few active region fields are present, and emerging at progressively lower latitudes until, at "solar maximum," they emerge near the equator. Over an 11-year cycle, approximately 10^{24} Mx of active region flux may emerge (Parker 1984).

The fate of active-region fields after emergence is unclear: observations have demonstrated that active region flux diffuses over the photosphere, and that magnetic features associated with active region fields can erupt from the solar surface. And some researchers believe active region fields can also "submerge" beneath the photosphere. Bipolar active region fields are not randomly oriented: an imaginary line joining the centers of the opposite polarities would run roughly in an east-west direction. The western-most flux in each bipole lies in the direction of the Sun's rotation, and can thus be termed the "leading polarity" in each bipole. *Hale's law* states that the leading polarities within one hemisphere are the same, while the leading polarities in the different hemispheres are opposites, and, further, that the leading polarities flip sign every 11 years.

These and other "regular" properties of active region fields have led to a near consensus among solar physicists that active region fields are generated by a *solar dynamo* operating beneath the photosphere, probably near the base of the convection zone, at $\sim .7R_{\odot}$. The precise workings of this dynamo are, however, not understood at this time.

We now contrast these properties of active region fields with the properties of quiet sun fields. Typical quiet sun magnetic elements contain much less flux than active region fields ($\lesssim 10^{19}$ Mx) and have much weaker average field strengths, on the order of tens of gauss. Their smaller size prevented observations of these fields

until the development of spectroscopic techniques over the previous century. In fact, only recently have high-resolution imaging techniques allowed solar physicists to begin characterizing the statistical properties of quiet-sun fields.

Few patterns are apparent in the spatial distribution and temporal evolution of quiet-sun magnetic fields. On the scale of the Sun's surface, their spatial distribution appears essentially uniform. At smaller scales, they are more common near the edges of *supergranules*, the large-scale (15-30 Mm) photospheric manifestation of upwellings in the convection zone. Observational studies demonstrating variations in quiet sun magnetic fields with the solar cycle are lacking; apparently, quiet sun fields come and go independently of the solar cycle. Using a lower-limit of 10^{18} Mx to define a quiet-sun magnetic flux element (Lin & Rimmele [1999] report lower flux fields, at the smallest spatial scales and fields strengths currently observable), rough estimates put $N \sim 10^4$ on the Sun's surface at any time (Hagenaar et al. 1999). Published estimates (Schrijver et al. 1997) suggest that all the flux in the quiet sun might be "cancelled" every $\sim$ 40 hours. If the fields replacing the cancelled fields are "new," and not just re-emerging fields that emerged and submerged at a previous time, then $\sim 10^{25}$ Mx of flux emerges in the quiet sun over an 11-year solar cycle, comparable to the whole-cycle active-region flux emergence rate.

The lack of readily discernable patterns in quiet sun fields' spatial and temporal

variability have led some solar physicists to speculate that quiet sun fields are generated in a "surface dynamo" operating in the upper convection zone (Cattaneo 1999). Another hypothesis is that quiet sun fields are merely the "reprocessed" remnants of active region fields that underwent diffusion in the turbulent flows of the upper convection zone.

This work concerns itself with quiet sun fields, and, in particular, the flux of *magnetic helicity* in quiet sun fields.

What is Magnetic Helicity?

Magnetic helicity $\mathcal{H}_M$ is defined as

$$\mathcal{H}_M \equiv \int_V d^3x \, \mathbf{A} \cdot \mathbf{B} \ , \tag{1.1}$$

where $\mathbf{B}$ is the magnetic field, $\mathbf{A}$ is the magnetic vector potential, $\mathbf{B} = \nabla \times \mathbf{A}$. To be gauge-invariant, the volume of integration V must be bounded by a "magnetic surface" S, on which $\mathbf{B}$ has no component along $\hat{n}$, the normal to S, i.e., $\mathbf{B} \cdot \hat{n}|_S = 0$. This integral quantifies the linkages among all pairs of field lines; it is a measure of the topological complexity of a given magnetic field.

To build a mental concept corresponding to this rather abstract mathematical expression, it is helpful to consider the magnetic helicity in the special case of two

thin magnetic flux tubes, of flux Φ_1 and Φ_2, immersed in field-free plasma. The vanishing divergence of the magnetic field, $\nabla \cdot \mathbf{B} = \mathbf{0}$, implies that each of these flux tubes forms a closed loop. We assume that field lines within each tube are untwisted, and, further, that flux tube 1 lies in a plane. In this idealized case, each flux tube can be envisioned as a closed loop of rope, with a sense of "direction" along each strand given by its magnetic field. Then, if the "ropes" are linked once, the integral in equation (1.1) is simple, and $\mathcal{H}_M = \pm 2\Phi_1\Phi_2$. The factor of 2 arises because the flux tubes are "mutually linked": if Φ_1 links Φ_2 once, Φ_2 must also link Φ_1 once.

The sign is determined by a "right hand rule" sense of linkage. We illustrate this idea by introducing the related concept of *crossings*: from any observer's point of view, two ropes that are linked will necessarily cross each other – one rope being "in front of" the other – at some points. (But ropes that cross each other are not necessarily linked!) Each crossing can be given a handedness: if the thumb of an observer's right hand points in the direction of rope 2 where rope 2 crosses rope 1, the crossing will be "right-handed" if the fingers of the right hand point in the same direction as rope 1, and "left-handed" if the fingers of the right hand point in the opposite direction to rope 1. Equivalently, crossings can be given a sign: a right-handed crossing is positive, while a left-handed crossing is negative. The linking number is the sum of all signed crossings the observer sees, divided by two.

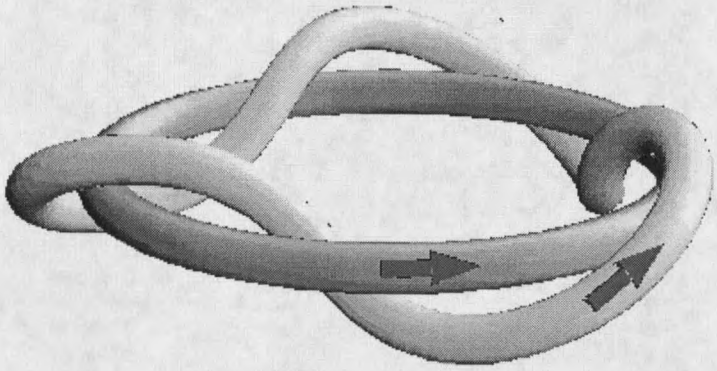

Figure 1.1: Two Linked Flux Tubes. In this case, the tubes have a linking number of -3 and mutual helicity of $-6\Phi_1\Phi_2$. *Illustration courtesy of M. Berger.*

If we had not assumed the field lines within each tube to be untwisted, the integral in equation (1.1) would also include "self" helicity contributions from the field-line linkages *within* each flux tube, in addition to the "mutual" helicity *between* the distinct flux tubes we computed above.

A drawing two flux tubes with a linking number of -3 and mutual helicity of $-6\Phi_1\Phi_2$ in figure 1.1 illustrates the concepts outlined here.

In many real-world situations, however, magnetic fields are not confined in flux tubes, and the integral in equation (1.1) in such cases can be non-trivial. But one property of fields that have non-zero magnetic helicity can still be intuitively understood: field lines in such cases have a *net* (as opposed to *gross*) *global* (as opposed to *local*) sense of *twist*.

More detailed discussions of magnetic helicity may be found in Moffatt (1978) and Berger & Field (1984).

Why Study the Transport of Magnetic Helicity?

In the magnetohydrodynamic approximation (Choudhuri 1998), the time evolution of a magnetic field is described by the induction equation,

$$\frac{\partial \mathbf{B}}{\partial t} = \nabla \times (\mathbf{v} \times \mathbf{B}) + \eta \nabla^2 \mathbf{B} \quad , \tag{1.2}$$

where η is the magnetic diffusivity $c^2/4\pi\sigma$, and σ is the electric conductivity.

In an *ideal* plasma, the conductivity is assumed infinite, meaning the magnetic diffusivity vanishes. In plasmas as hot as those in the Sun, this is a very reasonable approximation. Then the simplified induction equation,

$$\frac{\partial \mathbf{B}}{\partial t} = \nabla \times (\mathbf{v} \times \mathbf{B}) \quad , \tag{1.3}$$

implies that the magnetic field is "frozen in" to the plasma, and the topology of field lines is invariant. Since the magnetic helicity quantifies the topological linkages in a given field, the helicity is invariant ($d\mathcal{H}_M/dt = 0$) if the topology is. In fact, in magnetized plasmas which are highly conductive, but not perfectly so, magnetic helicity is still approximately conserved, even though other ideal invariants, notably field line topology, are not (Taylor 1974). *Hence, even during episodes of magnetic reconnection, magnetic helicity is essentially not destroyed,*

only redistributed.

Consequently, models meant to explain the evolution of solar magnetic fields must satisfy the constraint imposed by the approximate conservation of magnetic helicity. This has implications in many areas of current research in solar physics, including dynamo modeling, theories of coronal heating, research into flare triggers, the ultimate fate of active region flux, and *in situ* measurements of solar wind properties.

In the area of dynamo modelling, Boozer has pointed out in numerous papers (see his 1999 review) that the usual equations of a standard model for dynamos, called the mean-field dynamo theory, are inconsistent with the approximate conservation of magnetic helicity. He suggests that a correct treatment of the problem includes a helicity flux term, $\nabla \cdot \tilde{\mathbf{h}}$, where $2\tilde{\mathbf{h}}$ is the flux of magnetic helicity via the small-scale flow field. He also observes that two dynamos of equal but opposite helicity might form one "double dynamo" in the Sun. Presumeably, whatever helicity does not cancel in this way must be transported away from the Sun. Hence, a flux of helicity through the solar surface would be observed.

The flux of magnetic helicity might be related to coronal heating processes. Seehafer (Seehafer 1994) has suggested that coriolis-induced *kinetic helicity* in the flow field,

$$\mathcal{H}_K \equiv \int dV\, \mathbf{v} \cdot (\nabla \times \mathbf{v}), \tag{1.4}$$

can impart *current helicity*,

$$\mathcal{H}_C \equiv \int dV\, \mathbf{B} \cdot (\nabla \times \mathbf{B}), \tag{1.5}$$

to small-scale magnetic fields which initially contained no currents, $\mathbf{J} = c(\nabla \times \mathbf{B})/4\pi = 0$. Since fields with currents have more energy than current-free fields, or "potential" fields (so called because $\nabla \times \mathbf{B} = \mathbf{0}$ implies $\mathbf{B}$ can be written as the gradient of a scalar potential), the presence of current helicity implies the presence of free energy in the field. The presence of free energy in the field, in turn, has implications for coronal heating: the well-known "magnetic carpet" model of coronal heating (Schrijver et al. 1998), for instance, relies upon resistive dissipation of these currents to heat the corona. While general relationships between current and magnetic helicities are not known, Berger (1993) has demonstrated a correlation between the buildup of magnetic helicity and energy in one study. So the magnetic helicity flux through photosphere might be a proxy for the flux of energy through the photosphere.

In addition, the propagation of helicity (as a proxy for twist) in the solar atmosphere might have implications for triggering eruptive flares. Canfield & Reardon (1998) present intriguing observations that suggest reconnection might have been injecting twist into a magnetic flux system that later erupted from the solar surface

in a process that might be termed "helicity pumping." Canfield and collaborators have pursued this line of inquiry by studying both twist propagation (Jibben & Canfield 2001) and pre-eruptive reconnection (Colman & Canfield 2001) in Hα data.

The presence of structure, or lack of it, in the flux of magnetic helicity at the photosphere might also bear on the question of the ultimate fate of active region flux. Observations clearly show active region magnetic fields diffusing spatially and weakening with time after they emerge (see, e.g., Leighton [1964]); but this diffusion and weakening could arise from flux submergence or eruption, or from "eddy diffusivity" in turbulent plasma flows, or from anomalous resistivity at the molecular level, or from other processes, or from combinations of these mechanisms. If the flux of magnetic helicity in smaller, quiet-sun fields were found to possess the same well-characterized latitudinal, longitudinal, and temporal dependencies as active region fields, one plausible interpretation of this result would be that quiet sun fluxes are the remnants of decayed active region fields.

Finally, the flux of magnetic helicity in the solar wind can be compared to observations of magnetic helicity flux from the Sun. At the largest scale, Bieber *et al.*(1987) have characterized the magnetic helicity in the Parker spiral, which they find to be largely insensitive to the distribution of magnetic fields on the Sun. On an intermediate scale ($\sim$ 1 AU), Rust & Kumar (1996) have investigated

the expected flux of helicity in ejected flux ropes. DeVore used their results to estimate a whole-cycle solar wind helicity flux of 10^{46} Mx^2, which he asserts is in good agreement with *in situ* observations of the magnetic helicity flux near 1 AU (DeVore 2000). Regarding smaller scales, Smith's (1999) review of *in situ* observations of magnetic field structure in the solar wind near 1 AU reports minimal evidence for the presence of magnetic helicity, whether from solar "sources" or via helicity injection in the interplanetary medium between the Sun and 1 AU. Consequently, a measured non-zero flux of magnetic helicity through the Sun's surface at small scales might raise interesting questions about helicity transport above the photosphere.

Current Research in Solar Magnetic Helicity Transport

Various authors have considered the flux of magnetic helicity from active regions, using both theoretical and observational techniques. DeVore (2000) constructs models of bipolar active regions, and studies the injection of magnetic helicity through the photosphere into the corona from the shear introduced by a model differential rotation profile. He then extrapolates from these results to calculate a whole-Sun, whole-cycle flux of magnetic helicity from active regions. By combining the flux rope model of Burlaga et al. (1981) with the results of Webb

& Howard (1994), who studied the occurrence rates of and average magnetic flux in coronal mass ejections (CMEs), DeVore infers a rate of active-region helicity flux in the solar wind comparable to his theoretical rate of magnetic helicity injection. Further, he asserts that his rate is consistent with the *in situ* measurements reviewed by Smith (1999).

Chae (2001) uses local correlation tracking (LCT) of magnetic features in a sequence of line-of-sight magnetograms of an active region to measure the helicity flux through the photosphere into the corona in that active region. He finds that the temporal evolution of the helicity flux rate is highly structured, with occasional excursions well above the rate predicted by DeVore (2000), and, interestingly, a significant oscillation in the helicity flux, in the range of 10^{-4} Hz.

Green (2001) and collaborators have tracked an active region over several solar rotations and estimated both the helicity injected by differential rotation and the helicity ejected by eruptions. No attempt was made to track individual features in their analysis.

The Present Contribution to the Study of Solar Magnetic Helicity Transport

In this work, we estimate the helicity flux from the photosphere into the corona arising from the evolution of quiet-sun magnetic fields. We define *quiet-sun mag-*

netic fields as those arising from flux elements of approximately the characteristic flux size 3×10^{18}Mx, observed by Schrijver et al. (1997). These flux elements are isolated and can be approximated as point sources or sinks of magnetic flux.

By tracking individual magnetic flux elements and the temporal evolution of their structure, we can make an *observational* estimate of the quiet-sun helicity flux. The expression for the helicity flux can be written as the sum of two terms, the "mutual" and "self" helicity fluxes. The mutual helicity flux arises from the rotation of distinct flux elements about each other. The self helicity flux arises from the rotation of field lines in an individual flux element about each other.

The bulk of this thesis is devoted to telling the "stories" of these two helicity fluxes.

For comparison, we also compute theoretical values of the helicity flux. We assume the dominant source of systematic magnetic helicity injection is the differential rotation of the photosphere, and base our predicted helicity flux solely on this effect. Detailed calculations are presented below.

One other possible systematic source of helicity injection, the coriolis-induced kinetic helicity in the turbulent photospheric flow field discussed above, has not previously been observed, much less thoroughly characterized. Simple scaling arguments, however, suggest that it plays only a minor rôle in the dynamics of the turbulent solar flow field (see Appendix A).

In Chapter 2, we outline our theoretical approach to measuring the fluxes of mutual and self-helicities. In Chapter 3, we detail the procedures used to analyze data and calculate the helicity fluxes. In Chapter 4, we make theoretical predictions for the helicity flux, and in Chapter 5 we present the results of our measurements and compare them to our predictions. In Chapter 6, we conclude with a discussion of possible interpretations our results, and their implications.

CHAPTER 2

THEORY OF HELICITY TRANSPORT

Relative Helicity, and Its Flux

Magnetic fields above the solar photosphere can extend below the photosphere, so the normal component of the magnetic field at the surface S defined by the photosphere does not, in general, vanish:

$$\mathbf{B} \cdot \hat{n}|_S \neq 0 \ . \tag{2.1}$$

For this reason, the expression given in equation (1.1) for magnetic helicity,

$$\mathcal{H}_M = \int_V d^3x \ \mathbf{A} \cdot \mathbf{B} \ , \tag{2.2}$$

is *not* gauge-invariant. We expect that real physical systems, however, *are* gauge-invariant. Consequently, the physical interpretation of $\mathcal{H}_M$ defined this way is not clear in the solar case, and in other cases where the normal component of the magnetic field does not vanish on the boundary surface of the volume of integration.

In response, Berger and Field (1984) defined a guage-invariant quantity they termed the *relative helicity* of a magnetic field $\mathbf{B}$ and a vector potential for that field, $\mathbf{A}$. Their method uses the difference between the helicity computed using $\mathbf{B}$ and $\mathbf{A}$, and the helicity calculated using the current-free magnetic field, $\mathbf{B}_P$, that matches $(\mathbf{B} \cdot \hat{n})|_S$, the normal component of the magnetic field $\mathbf{B}$ on the boundary surface S, and $\mathbf{A}_P$, a vector potential for $\mathbf{B}_P$. Hence, $\mathbf{B}_P$ and $\mathbf{A}_P$ are used as "reference" fields. Finn & Antonsen (1985) showed that this approach is equivalent to defining the relative helicity as

$$\mathcal{H}_{M_R} \equiv \int_V d^3x \; (\mathbf{A} + \mathbf{A}_P) \cdot (\mathbf{B} - \mathbf{B}_P) \; . \tag{2.3}$$

Essentially, the contribution to the total helicity from fields outside the boundary surface S cancels in this expression (see also, e.g., Berger 1999).

We digress to comment on the relative helicity of non-potential fields. The "potential magnetic field" $\mathbf{B}_P$ gets its name from its lack of current, $\mathbf{J}_P = \nabla \times \mathbf{B}_P = 0$, which means the magnetic field can be represented using a scalar potential χ, usually as $\mathbf{B}_P = -\nabla\chi$. Then the vanishing divergence of any magnetic field means χ satisfies Laplace's equation,

$$0 = \nabla \cdot \mathbf{B}_P = -\nabla^2\chi \; , \tag{2.4}$$

which has a unique solution for a given boundary condition. Any field $\mathbf{B}$ which carries a current is, therefore, "non-potential." This fact, with the definition in equation (2.3), means that *a given field* $\mathbf{B}$ *has a nonzero relative helicity if and only if it carries a current.*

Taking the time derivative of their expression for the relative helicity, and using the induction equation, (1.3), Berger and Field (1984) and Berger (1984) have derived a "Poynting" theorem for the flux of relative helicity through a surface S,

$$\frac{d\mathcal{H}_{M_R}}{dt} = 2\oint_S da\Big((\mathbf{A}\cdot\mathbf{B})\mathbf{v} - (\mathbf{A}_P\cdot\mathbf{v})\mathbf{B}\Big)\cdot\hat{n} \quad . \tag{2.5}$$

In this work, we study the flux of helicity in Cartesian geometry, taking photosphere to be a plane surface S located at $z = 0$. In this case, $\hat{n} = \hat{z}$, and we may rewrite the expression above as

$$\frac{d\mathcal{H}_{M_R}}{dt} = 2\int_S da\Big(\underbrace{(\mathbf{A}\cdot\mathbf{B})v_z}_{\text{"advection"}} - \underbrace{(\mathbf{A}_P\cdot\mathbf{v})B_z}_{\text{"braiding"}}\Big) \quad . \tag{2.6}$$

Flux of Magnetic Helicity via Advection

The "advection" term corresponds to the emergence or submergence of fields already containing magnetic helicity across the photosphere. Since the magnetic vector potential cannot be measured, it is also impossible to measure the rate of

magnetic helicity emergence directly.

Leka, et al. (1996), however, report observations of active-region magnetic flux, B_z, emerging through the photosphere carrying vertical current, J_z. These newly-emerged fields therefore possess non-zero current helicity (see equation [1.5]). Other observations also support the subphotospheric origin of observed current helicity in active-region fields observed at the photosphere, e.g., those of Pevstov et al. (1997). While the general relation between $\mathcal{H}_{M_R}$ and $\mathcal{H}_C$ is unclear, both are, in practice, commonly viewed as proxies for twist in fields. (In fact, sometimes the terms "magnetic helicity" and "current helicity" are used interchangeably, which is incorrect.) Hence, these observations have been taken to imply that active region fields containing nonzero *magnetic* helicity are advected into the corona (Chae 2001).

In this work, we are primarily concerned with quiet-sun magnetic fields, as opposed to active region magnetic fields. Unlike observations of active-region fields, observations of quiet-sun (Pevtsov & Longcope 2001) fluxes only tentatively support models in which small-scale magnetic fields emerge with a systematic bias in helicity. Hence, we ignore the contribution to the total helicity flux arising from the advection term.

Flux of Magnetic Helicity via Braiding

Proceeding from the analysis in the previous section, we focus solely on the "braiding" term in equation (2.6) from now on, assuming

$$\frac{d\mathcal{H}_{M_R}}{dt} \simeq -2 \int_S da(\mathbf{A}_P \cdot \mathbf{v}) B_z \quad . \tag{2.7}$$

For simplicity, we now drop the subscript M_R: $\mathcal{H}$ refers to the relative magnetic helicity unless explicity stated otherwise.

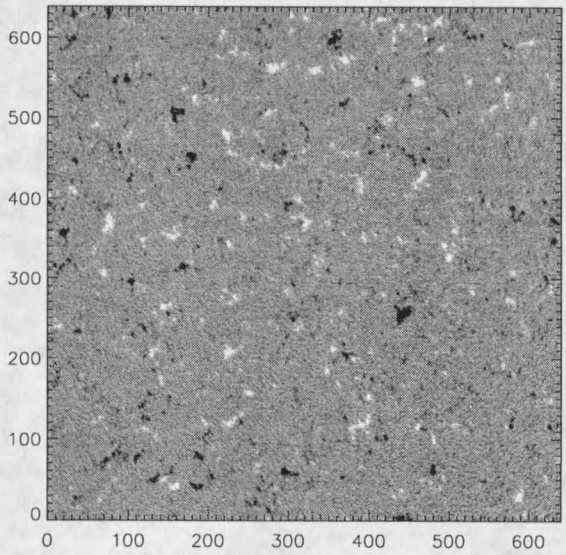

Figure 2.1: Quiet Sun Magnetic Fields in Isolated Regions. In this image of magnetic fields in the quiet sun, measured by SoHO-MDI, magnetic flux is seen only in small, isolated patches. Regions of positive magnetic flux are conventionally shown as white, while regions of negative magnetic flux are black.

Consider the image of line-of-sight magnetic fields at the Sun's photosphere in

figure 2.1, determined by inversion of the Stokes V profile (Rees, 1987; Jenkins & White, 1957) in a photospheric absorption line measured by the Michelson Doppler Imager (MDI) on the Solar and Heliospheric Observatory (SoHO) in its high-resolution ("hi res") mode (Scherrer et al. 1995). One can see that the magnetic field in this patch of quiet-sun is non-zero only in small, isolated regions. This means we can approximate the normal magnetic field B_z at the Sun's surface as arising from N "point-like" sources.

We define the normalized, flux-weighted average position of the ith source (its magnetic "center of flux") in the usual way,

$$\bar{\mathbf{x}}_i \equiv \frac{1}{\Phi_i} \int_S d^2x \, B_z \mathbf{x} \quad , \tag{2.8}$$

where S is the area covered by the ith source. Then

$$B_z(\mathbf{x}) = \sum_{i=1}^{N} \Phi_i \, \Delta_i(\mathbf{x} - \bar{\mathbf{x}}_i) \quad , \tag{2.9}$$

where $\Delta_i(\mathbf{x} - \bar{\mathbf{x}}_i)$ is the distribution of flux in the ith source, and is strongly peaked near $\bar{\mathbf{x}}_i$ and zero far away.

In Coulomb guage, the vector potential for the current-free magnetic field $\mathbf{B}_P$,

evaluated on the surface, is

$$\begin{aligned}
\mathbf{A}_P(\mathbf{x}) &= \frac{1}{2\pi}\int_S da' B_z(\mathbf{x}')\frac{\hat{z}\times(\mathbf{x}-\mathbf{x}')}{|(\mathbf{x}-\mathbf{x}')|^2} \\
&= \sum_{i=1}^{N}\frac{\Phi_i}{2\pi}\int_S da'\Delta_i(\mathbf{x}'-\mathbf{x}_i)\frac{\hat{z}\times(\mathbf{x}-\mathbf{x}')}{|(\mathbf{x}-\mathbf{x}')|^2} \qquad (2.10)\\
&= \sum_{i=1}^{N}\mathbf{A}_P^{(i)}(\mathbf{x}) \quad ,
\end{aligned}$$

where we have defined the vector potential due to the ith flux element, $\mathbf{A}_P^{(i)}$.

Inserting these expressions into equation (2.7), we have

$$\begin{aligned}
\frac{d\mathcal{H}}{dt} &= -2\int da(\mathbf{v}\cdot\mathbf{A}_P)B_z \\
&\simeq -2\int_S da\Big(\mathbf{v}\cdot\sum_{i=1}^{N}\mathbf{A}_P^{(i)}\Big)\Big(\sum_{j=1}^{N}\Phi_j\Delta_j(\mathbf{x}-\bar{\mathbf{x}}_j)\Big) \quad . \qquad (2.11)
\end{aligned}$$

One can treat the $i=j$ term in the double summation separately, resulting in an expression for the helicity flux with "self" and "mutual" terms,

$$\begin{aligned}
\frac{d\mathcal{H}}{dt} \simeq\ & \underbrace{-2\sum_{i=1}^{N}\Phi_i\int_S da(\mathbf{v}\cdot\mathbf{A}_P^{(i)})\Delta_i(\mathbf{x}-\bar{\mathbf{x}}_i)}_{\text{“self”}} \qquad (2.12)\\
&+ \underbrace{\Big(-\sum_i\sum_{j\neq i}\Phi_j\int_S da(\mathbf{v}\cdot\mathbf{A}_P^{(i)})\Delta_j(\mathbf{x}-\bar{\mathbf{x}}_j)}_{\text{“mutual”}} \quad .
\end{aligned}$$

Theory of "Mutual Helicity" Transport

We treat the mutual helicity term in equation (2.12) first, since it is most easily evaluated. Since $i \neq j$ by assumption in the mutual helicity flux term, we are dealing with distinct fluxes, and we can approximate the flux distribution functions Δ_i with δ-functions,

$$B_z(\mathbf{x}) \simeq \sum_{i=1}^{N} \Phi_i \, \delta(\mathbf{x} - \bar{\mathbf{x}}_i) \, . \tag{2.13}$$

Writing out the $\mathbf{A}_P^{(i)}$ term in (2.12) using (2.10), we have

$$\begin{aligned} \mathbf{A}_P^{(i)}(\mathbf{x}) &= \frac{\Phi_i}{2\pi} \int_S da' \Delta_i(\mathbf{x}' - \bar{\mathbf{x}}_i) \frac{\hat{z} \times (\mathbf{x} - \mathbf{x}')}{|(\mathbf{x} - \mathbf{x}')|^2} && (2.14) \\ &\simeq \frac{\Phi_i}{2\pi} \int_S da' \delta(\mathbf{x}' - \bar{\mathbf{x}}_i) \frac{\hat{z} \times (\mathbf{x} - \mathbf{x}')}{|(\mathbf{x} - \mathbf{x}')|^2} \\ &= \frac{\Phi_i}{2\pi} \frac{\hat{z} \times (\mathbf{x} - \bar{\mathbf{x}}_i)}{|(\mathbf{x} - \bar{\mathbf{x}}_i)|^2} \, . && (2.15) \end{aligned}$$

Thus, the vector potential due to ith source is circumferential in this approximation, as illustrated in figure 2.2.

Then the full expression for the mutual helicity becomes

$$\begin{aligned} \frac{d\mathcal{H}^{(\mathrm{MUT})}}{dt} &\simeq -\sum_i \sum_{j \neq i} \frac{\Phi_i \Phi_j}{\pi} \int_S da \frac{(\mathbf{v} \cdot \hat{z} \times (\mathbf{x} - \bar{\mathbf{x}}_i))}{|(\mathbf{x} - \bar{\mathbf{x}}_i)|^2} \delta(\mathbf{x} - \bar{\mathbf{x}}_j) \\ &= -\frac{1}{\pi} \sum_i \sum_{j \neq i} \Phi_i \Phi_j \Omega_{ij} \, , && (2.16) \end{aligned}$$

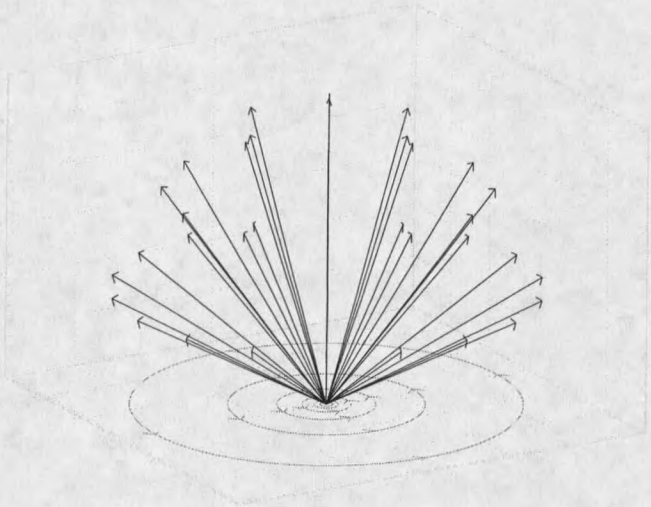

Figure 2.2: Circumferential Vector Potential. A point source of positive magnetic flux situated at the origin and its azimuthal vector potential are shown here. The dark lines which radiate from the origin are magnetic field lines, while the light, circular lines on the bottom plane are tangent lines of the vector potential evaluated on that surface.

where

$$\Omega_{ij} \equiv \Big(\mathbf{v}(\bar{\mathbf{x}}_j) - \mathbf{v}(\bar{\mathbf{x}}_i)\Big) \cdot \frac{\hat{z} \times (\bar{\mathbf{x}}_j - \bar{\mathbf{x}}_i)}{|(\bar{\mathbf{x}}_j - \bar{\mathbf{x}}_i)|^2} \tag{2.17}$$

is the angular velocity of the jth flux element about the ith. Thus we can define the mutual helicity flux from each *pair* of fluxes as

$$\frac{d\mathcal{H}_{ij}}{dt} \equiv -\frac{2}{\pi}\Phi_i\Phi_j\Omega_{ij} \quad , \tag{2.18}$$

where the factor of two arises from the double summation.

It is now obvious how the circumferential vector potential $\mathbf{A}_P^{(i)}$ from the ith

flux, found in equation (2.15), combined with the rotation Ω_{ij} of the jth flux about the location $\bar{\mathbf{x}}_i$ of the ith flux, gives rise to a nonzero $(\mathbf{v} \cdot \mathbf{A}_P)$ term in equation (2.7). Hence, a flux of magnetic helicity results from the winding of one flux about another.

The negative sign means that winding a pair of oppositely-signed fluxes in the right-hand sense leads to a *positive* flux of helicity, while right-handed braiding of two fluxes of the same sign causes a *negative* flux of helicity. This can be understood by considering the handedness of the crossings (see Chapter 1) introduced in the cartoon models of these two processes illustrated in figure 2.3.

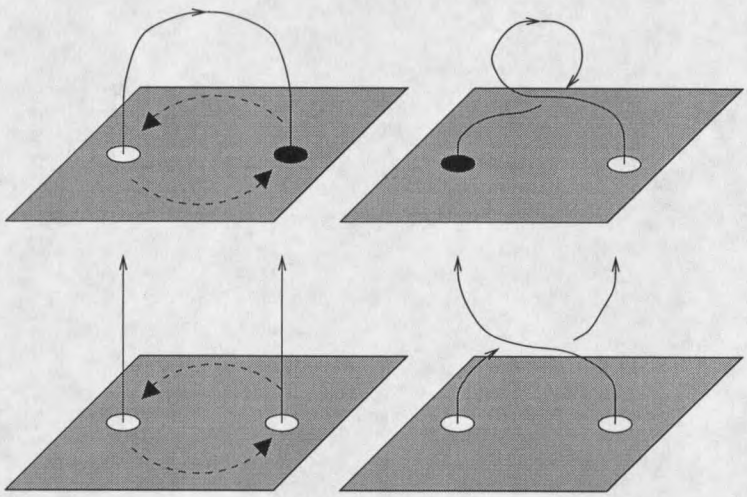

Figure 2.3: Sign of Mutual Helicity Flux. Winding footpoints in the right-hand sense can lead to a flux of positive helicity (top row) or a flux of negative helicity (bottom row), depending on the sign of fluxes involved in the braiding.

Applicability to the Sun

Do fluxes wind about each other on the Sun? Yes, via the differential rotation of the photosphere: the angular velocity of the photospheric equator about the Sun's axis of rotation exceeds the angular velocities at higher latitudes, systematically winding magnetic fluxes at different latitudes about each other. Figure 2.4 illustrates this partial winding: points initially along a single meridian of longitude (marked with $\diamond$'s) in the Sun's northern hemisphere are mapped (to points marked with $\times$) over one mid-latitude rotation in accordance with the differential rotation profile of Snodgrass (1984). To an observer $\times$, the poleward and equator-ward $\times$'s appear to have rotated about her position in a right-hand sense, with respect to an *outward* normal vector on the Sun's surface.

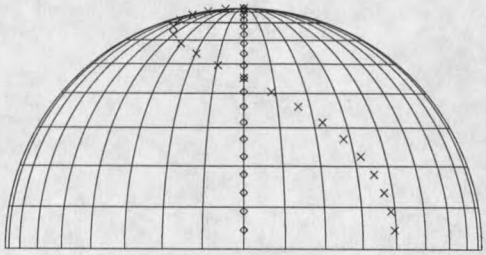

Figure 2.4: Differential Rotation Braids Footpoints. Points at different latitudes wind partially around each other, as illustrated in this mapping ($\diamond \rightarrow \times$) over one mid-latitude rotation. The relative rotation is in a right-hand sense with respect to an *outward* normal vector.

Other systematic properties of the flow field at the photosphere are expected to make significantly smaller contributions to the flux of mutual helicity, and are

not considered in our study.

Theory of "Self Helicity" Transport

We now attack the term in equation (2.12) representing the flux of "self helicity," which will involve much more effort than analysis of the mutual helicity term did.

From equation (2.12), the self helicity term is

$$\frac{d\mathcal{H}^{(\mathrm{SELF})}}{dt} \simeq -2\sum_{i=1}^{N}\Phi_i\int_S da(\mathbf{v}\cdot\mathbf{A}_P^{(i)})\Delta_i(\mathbf{x}-\bar{\mathbf{x}}_i) \tag{2.19}$$

$$\simeq -\frac{1}{\pi}\sum_i\Phi_i^2\int_S da\left(\mathbf{v}\cdot\frac{\hat{z}\times(\mathbf{x}-\bar{\mathbf{x}}_i)}{|(\mathbf{x}-\bar{\mathbf{x}}_i)|^2}\right)\Delta_i(\mathbf{x}-\bar{\mathbf{x}}_i)\ , \tag{2.20}$$

where we have employed the "point-like" approximation used in equation (2.15) to evaluate $\mathbf{A}_P^{(i)}$, but kept the general form of the normal flux distribution, $B_z^{(i)} = \Phi_i\Delta_i(\mathbf{x}'-\mathbf{x}_i)$, for evaluation of the integral over S.

We now analyze the ith term in the series, to generalize the result to all terms. Accordingly, we drop the subscript i and refer to the ith flux as simply "the flux."

To investigate the structure of $\Delta(\mathbf{x}-\bar{\mathbf{x}})$ for $\mathbf{x}$ near $\bar{\mathbf{x}}$, we define a local cylindrical polar coordinate system centered on $\bar{\mathbf{x}}$, viz.,

$$\delta\mathbf{x} \equiv (\mathbf{x}-\bar{\mathbf{x}}) \tag{2.21}$$

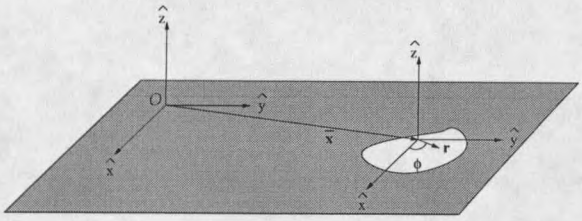

Figure 2.5: Coordinates from Center of Flux. Cylindrical polar coordinates centered at $\bar{\mathbf{x}}$, the magnetic center-of-flux.

$$r \equiv |\delta\mathbf{x}| \tag{2.22}$$

$$\phi \equiv \sin^{-1}(\hat{z}\cdot(\hat{x}\times\delta\mathbf{x})) \ . \tag{2.23}$$

Assuming the velocity field is smooth near $\bar{\mathbf{x}}$, one can write

$$\mathbf{v}(\mathbf{x}) \simeq \mathbf{v}(\bar{\mathbf{x}}) + \mathbf{M}(\bar{\mathbf{x}})\cdot\delta\mathbf{x} \ , \tag{2.24}$$

where $\mathbf{M}(\bar{\mathbf{x}})$ is the Jacobian matrix,

$$M_{ij}(\bar{\mathbf{x}}) = \left.\frac{\partial v_i}{\partial x_j}\right|_{\bar{\mathbf{x}}} \ , \tag{2.25}$$

where x_i and x_j here refer to the local coordinate axes $x_1 = x$ and $x_2 = y$.

Then the self helicity flux is given by

$$\frac{dH^{(\mathrm{SELF})}}{dt} = -\frac{\Phi^2}{\pi}\Bigg[\underbrace{\int_S da\frac{\Delta(\mathbf{x})(\hat{z}\times\delta\mathbf{x})\cdot\mathbf{v}(\bar{\mathbf{x}})}{|\delta\mathbf{x}|^2}}_{I}$$

$$+ \underbrace{\int_S da \frac{\Delta(\mathbf{x})(\hat{z} \times \delta\mathbf{x})}{|\delta\mathbf{x}|^2} \cdot \Big(\mathbf{M}(\bar{\mathbf{x}}) \cdot \delta\mathbf{x}\Big)}_{II} \Bigg] . \tag{2.26}$$

Writing $I.$ in cylindrical coordinates gives

$$I. = \int_0^\infty dr \frac{r^2}{r^2} \int_0^{2\pi} d\phi \Delta(\mathbf{x})(\cos\phi\hat{x} + \sin\phi\hat{y}) \cdot (\mathbf{v}(\bar{\mathbf{x}}) \times \hat{z}) \ . \tag{2.27}$$

One can write the the magnetic flux-distribution function $\Delta(\mathbf{x})$ as an expansion in (r, ϕ) using functions which are orthogonal in the azimuthal coordinate ϕ,

$$\Delta(\mathbf{x}) = \Delta(r, \phi) = \frac{1}{2} f_0(r) + \sum_{n=2}^{\infty} f_n(r)\cos(n\phi) + g_n(r)\sin(n\phi) \ , \tag{2.28}$$

where terms with $n > 0$ quantify the distribution's departure from axisymmetry. Incidentally, we note that equation (2.9) implies that $\Delta(\mathbf{x})$ has units of inverse area, which means f_n and g_n also have units of [length]$^{-2}$.

From equation (2.9) we also know that the radial integral of the "zeroth-order" term in the series must be normalized. This follows from

$$\Phi \equiv \int da \ B_z(\mathbf{x}) \tag{2.29}$$

$$= \int da \ \Phi\Delta(\mathbf{x}) \tag{2.30}$$

$$= \Phi \int_0^{2\pi} d\phi \int_0^\infty dr \, r\Delta(r, \phi) \tag{2.31}$$

$$= \frac{1}{2}\Phi(2\pi)\int_0^\infty dr\, r f_0(r) \tag{2.32}$$

$$\Longrightarrow 1 = \underbrace{\pi\int_0^\infty dr\, r f_0(r)}_{\equiv F_0^{(1)}}\,, \tag{2.33}$$

where we have defined

$$F_n^{(m)} \equiv \pi\int_0^\infty dr\, r^m f_n(r)\,. \tag{2.34}$$

We define $G_n^{(m)}$ analogously.

To find $f_n(r)$ for $n > 0$, we multiply equation (2.28) by $\cos(n\phi)$, and use equation (2.9) to integrate B_z over $\phi \in [0, 2\pi]$, which gives, via the functions' orthogonality,

$$\Phi f_n(r)\int_0^{2\pi} d\phi\cos^2(n\phi) = \int_0^{2\pi} d\phi B_z(r,\phi)\cos(n\phi) \tag{2.35}$$

$$(\pi\Phi) f_n(r) = \int_0^{2\pi} d\phi B_z(r,\phi)\cos(n\phi) \tag{2.36}$$

$$\Longrightarrow f_n(r) = \frac{1}{(\pi\Phi)}\int_0^{2\pi} d\phi B_z(r,\phi)\cos(n\phi)\,. \tag{2.37}$$

Equation (2.37) also yields the correct result for $f_0(r)$. Substitution of $f_n(r) \to g_n(r)$ and $\cos(n\phi) \to \sin(n\phi)$ in the equations above yields an analogous result for $g_n(r)$. Using equation (2.34), we have

$$F_n^{(m)} = \pi\int_0^\infty dr\, r^m \frac{1}{(\pi\Phi)}\int_0^{2\pi} d\phi B_z(r,\phi)\cos(n\phi) \tag{2.38}$$

$$= \frac{1}{\Phi}\int_0^\infty dr\, r^m \int_0^{2\pi} d\phi B_z(r,\phi)\cos(n\phi)\ , \tag{2.39}$$

and similarly for $G_n^{(m)}$. The units of $F_n^{(m)}$ and $G_n^{(m)}$ are $[\text{length}]^{(m-1)}$.

We digress to consider the first few "higher order" coefficients in this series. Both f_1 and g_1 are zero, as may be seen by writing

$$\begin{aligned}
0 &\equiv \frac{1}{\Phi}\int_0^\infty dr\, r \int_0^{2\pi} d\phi\, B_z \delta\mathbf{x} && (2.40)\\
&= \int_0^\infty dr\, r^2 \int_0^{2\pi} d\phi\, \Delta(\mathbf{x})(\cos(\phi)\hat{x} + \sin(\phi)\hat{y}) \\
&= \int_0^\infty dr\, r^2 \int_0^{2\pi} d\phi\, (\frac{1}{2}f_0 + f_1\cos(\phi) + g_1\sin(\phi))(\cos(\phi)\hat{x} + \sin(\phi)\hat{y}) \\
&= \int_0^\infty dr\, r^2 \int_0^{2\pi} d\phi\, (\frac{1}{2}f_0(r))(\cos(\phi)\hat{x} + \sin(\phi)\hat{y}) \\
&+ \int_0^\infty dr\, r^2 \int_0^{2\pi} d\phi\, f_1\cos(\phi)(\cos(\phi)\hat{x} + \sin(\phi)\hat{y}) \\
&+ \int_0^\infty dr\, r^2 \int_0^{2\pi} d\phi\, g_1\sin(\phi)(\cos(\phi)\hat{x} + \sin(\phi)\hat{y}) \\
&= \pi\int_0^\infty dr\, r^2 (f_1\hat{x} + g_1\hat{y})\ . && (2.41)
\end{aligned}$$

Returning now to equation (2.26) to evaluate $I.$, we see that the "zeroth order" contribution vanishes,

$$I.^{(0)} = \frac{1}{2}\int_0^\infty dr\, f_0(r)\int_0^{2\pi} d\phi(v_y(\bar{\mathbf{x}})\cos\phi - v_x(\bar{\mathbf{x}})\sin\phi) = 0\ . \tag{2.42}$$

Hence, motion of the magnetic "center of flux" causes no flux of helicity.

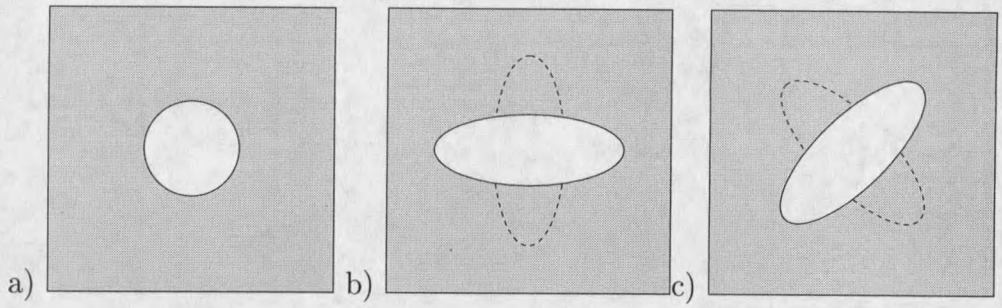

Figure 2.6: Flux Shapes. Different flux distributions have different expansion coefficients: a) an axisymmetric flux distribution: $F_2^{(m)} = 0 = G_2^{(m)}$; b) white area has $F_2^{(m)} > 0$, while area within dashes has $F_2^{(m)} < 0$; c) white area has $G_2^{(m)} > 0$, while area within dashes has $G_2^{(m)} < 0$.

Next, since f_1 and g_1 are zero, there are no "first order" contributions to I. Finally, at "second order," all angular integrations contain a triple product of sines and/or cosines, and therefore vanish.

Moving on to evaluate $II.$ in equation (2.26), rewriting the integral in component notation (with implied summation) gives

$$II. = \int_S d^2x \frac{\Delta(\mathbf{x})(\delta x_i \hat{x}_j \epsilon_{ij3})}{\delta x^2}(M_{kl}\hat{x}_k\hat{x}_l)(\delta x_m \hat{x}_m) \tag{2.43}$$

$$= \int_S d^2x \frac{\Delta(\mathbf{x})(\delta x_i)(\delta x_m) M_{jm}\epsilon_{ij3}}{\delta x_k \delta x_k} . \tag{2.44}$$

Adopting cylindrical coordinates and employing the expansion (2.28) gives, at "zeroth order,"

$$II.^{(0)} = \frac{1}{2}\int_0^\infty dr \frac{r^3}{r^2} f_0(r) \int_0^{2\pi} d\phi \left(\frac{\partial v_y}{\partial x}\cos^2(\phi) - \frac{\partial v_x}{\partial y}\sin^2(\phi) \right) \tag{2.45}$$

$$= \frac{\pi}{2}\left(\frac{\partial v_y}{\partial x} - \frac{\partial v_x}{\partial y}\right)\int_0^\infty dr \frac{r^3}{r^2} f_0(r) \tag{2.46}$$

$$= \frac{1}{2}\left(\frac{\partial v_y}{\partial x} - \frac{\partial v_x}{\partial y}\right) \tag{2.47}$$

$$= \omega_z(\bar{\mathbf{x}}) \ , \tag{2.48}$$

which is just the flux of self helicity due to the magnetic source's rotation about its own axis. In the last line, we have used the definition

$$\omega_z = \frac{1}{2}(\nabla \times \mathbf{v})_z. \tag{2.49}$$

As with with $I.^{(2)}$, the angular integrations in the "first order" contribution here, $II.^{(1)}$, are triple products of sines and cosines, and therefore vanish.

The "second order" contribution is

$$\begin{aligned} II.^{(2)} &= \int_0^\infty dr\, r \int_0^{2\pi} d\phi \left[f_2 \cos(2\phi) + g_2 \sin(2\phi)\right] h_k(\phi) h_m(\phi)(\epsilon_{kl3} M_{lm}) \\ &= \int_0^\infty dr\, r \int_0^{2\pi} d\phi\, f_2 \cos^2(\phi) h_k(\phi) h_m(\phi)(\epsilon_{kl3} M_{lm}) \\ &- \int_0^\infty dr\, r \int_0^{2\pi} d\phi\, f_2 \sin^2(\phi) h_k(\phi) h_m(\phi)(\epsilon_{kl3} M_{lm}) \\ &+ \int_0^\infty dr\, r \int_0^{2\pi} d\phi\, 2 g_2 \sin(\phi)\cos(\phi)) h_k(\phi) h_m(\phi)(\epsilon_{kl3} M_{lm}) \ , \end{aligned} \tag{2.50}$$

where $h_1(\phi) \equiv \cos(\phi)$, and $h_2(\phi) \equiv \sin(\phi)$.

Evaluating the angular integrals and their coefficients gives:

Integral		Result	Coefficients
$\int_0^{2\pi} d\phi \, \cos^3(\phi)\sin(\phi)$	$=$	0	$-$
$\int_0^{2\pi} d\phi \, \sin^3(\phi)\cos(\phi)$	$=$	0	$-$
$\int_0^{2\pi} d\phi \, \cos^4(\phi)$	$=$	$3\pi/4$	$+f_2\epsilon_{123}M_{21}$
$\int_0^{2\pi} d\phi \, \sin^4(\phi)$	$=$	$3\pi/4$	$-f_2\epsilon_{213}M_{12}$
$\int_0^{2\pi} d\phi \, \cos^2(\phi)\sin^2(\phi)$	$=$	$\pi/4$	$+f_2\epsilon_{213}M_{12} - f_2\epsilon_{123}M_{21}$
			$+2g_2\epsilon_{123}M_{22} + 2g_2\epsilon_{213}M_{11}$

Combining like terms yields

$$
\begin{aligned}
II. &= \frac{\pi}{4}\int_0^\infty drr\Big(3f_2(M_{12}+M_{21}) \\
&+ -\Big(f_2(M_{12}+M_{21}) + 2g_2(M_{11}-M_{22})\Big)\Big) \qquad (2.51) \\
&= \pi\int_0^\infty drr\Big(f_2(M_{12}+M_{21})/2 - g_2(M_{11}-M_{22})/2\Big) . \qquad (2.52)
\end{aligned}
$$

The Jacobian matrix of the flow field M can be rewritten as

$$
\begin{pmatrix} M_{11} & M_{12} \\ M_{21} & M_{22} \end{pmatrix} = D\begin{pmatrix} 1 & 0 \\ 0 & 1 \end{pmatrix} + T\begin{pmatrix} 1 & 0 \\ 0 & -1 \end{pmatrix}
$$

$$+ \; C \begin{pmatrix} 0 & -1 \\ 1 & 0 \end{pmatrix} + X \begin{pmatrix} 0 & 1 \\ 1 & 0 \end{pmatrix} , \tag{2.53}$$

where

$$\begin{aligned} D &\equiv (M_{11} + M_{22})/2 \equiv \tfrac{1}{2}\mathrm{Tr(M)} && (\text{“divergence”}) \\ C &\equiv (M_{21} - M_{12})/2 \equiv \text{antisymmetric } = \omega_z && (\text{“curl”}) \\ T &\equiv (M_{11} - M_{22})/2 \equiv \text{traceless, diagonal} && (\text{“+”-flow}) \\ X &\equiv (M_{21} + M_{12})/2 \equiv \text{traceless, symmetric} && (\text{“x”-flow}) , \end{aligned} \tag{2.54}$$

and $M_{ij} \equiv \partial v_i / \partial x_j$.

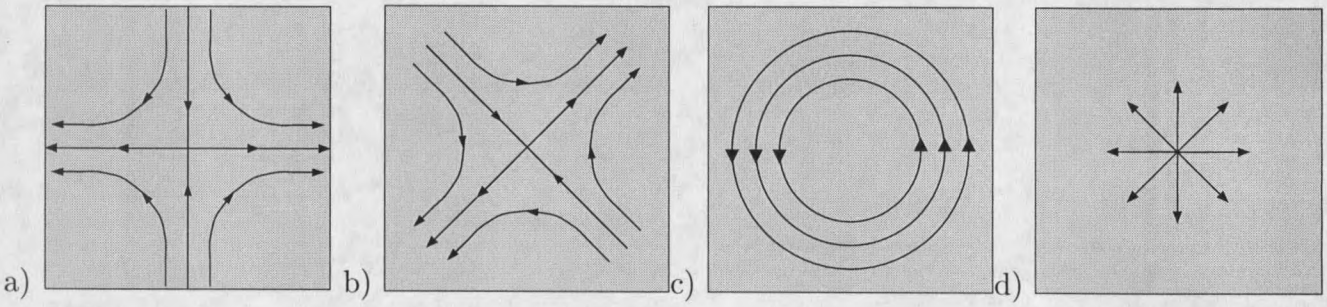

Figure 2.7: Elementary Flow Patterns. Any flow field can be locally represented in the comoving frame as the superposition of these four “elementary” flows: a) “+” flow, a stagnation flow aligned with axes; b) “x” flow, as previous case, but with flow axes tilted; c) “curl” flow, with nonzero vorticity; d) “diverging” flow, with nonzero divergence.

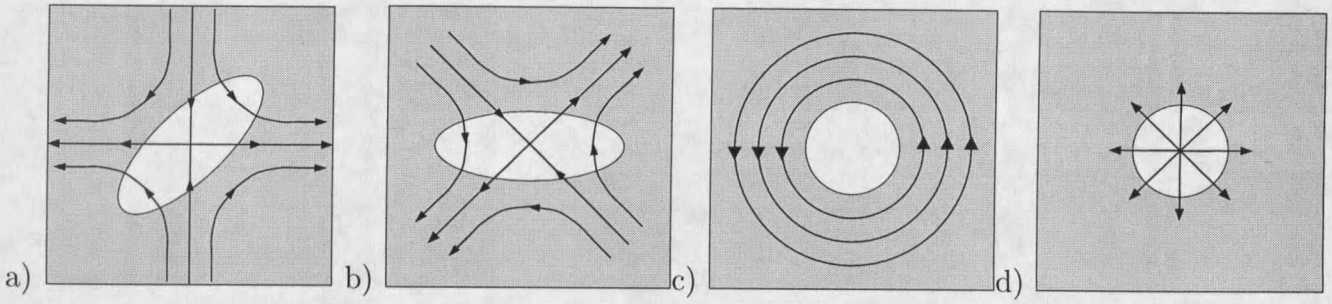

Figure 2.8: Flux Distributions Combined With Flows "Generate" Helicity. Some flows "generate" self helicity: a) "+" flow aligned with axes and non-axisymmetric flux distribution tilted off axes; b) "x" flow tilted off axes and aligned but non-axisymmetrix flux distribution; c) "curl" flow about center of *arbitrary* flux distribution. d) While "diverging" flow does not imply helicity generation, it might signal helicity advection.

Then the helicity flux can be written as

$$\frac{dH^{(\mathrm{SELF})}}{dt} = -\frac{\Phi^2}{\pi}\left(C + \pi\left(X\int_0^\infty dr\, r\, f_2(r) - T\int_0^\infty dr\, r\, g_2(r)\right)\right) \tag{2.55}$$

$$= -\frac{\Phi^2}{\pi}\left(C + \left(XF_2^{(1)} - TG_2^{(1)}\right)\right) . \tag{2.56}$$

Applicability to the Sun

Do systematic properties of the Sun's flow field tend to wind a given flux about its own axis? Perhaps shear from the differential rotation might cause systematic winding in individual flux elements, as might coriolis-induced handedness in the photospheric flows, if present.

The efficacy of either mechanism at winding field lines depends on both the magnetic diffusivity of the photospheric plasma, and the strength of the magnetic

field relative to the gas pressure. If the magnetic diffusivity is sufficiently high, then magnetic field lines are not "frozen in," and magnetic field can ignore the presence of a given flow pattern in the photospheric gas. And if the magnetic pressure $p_M = B^2/8\pi$ is much stronger than the gas pressure $p_G = nkT$, then any flow of photospheric gas will not exert sufficient force to affect the magnetic field. But we do not observe rapid diffusion of magnetic fields at the photosphere, and infer that the magnetic diffusivity at the photosphere is low. Further, the ratio of the pressures, $\beta \equiv p_G/p_M$, is of order unity at the photosphere, meaning magnetic flux concentrations should feel some effects from fluid motions in their vicinity. Finally, observations of the advection of magnetic flux concentrations by photospheric flows support the idea that photospheric magnetic features are strongly influenced by flows in the plasma in which they are immersed.

Differential rotation, or a non-vanishing latitudinal gradient in the rotation rate,

$$\frac{\partial \Omega}{\partial \theta} \neq 0 \ , \tag{2.57}$$

where θ is the colatitude, is equivalent to a shear flow about any point on the surface. In the plane tangent to an arbitrary point on the Sun's surface, adopting a right-hand coordinate system with $\hat{z}$ normal to the plane and $\hat{x}$ in the direction of the Sun's rotation (west in the plane of the Earth's sky, on the visible disk), the

differential rotation is equivalent to

$$0 \neq \frac{\partial v_x}{\partial y} = (X - C) \quad ; \tag{2.58}$$

in terms of the elemental flow patterns derived above. Hence, from equation (2.56), the flux of self helicity should not, for a general flux element, vanish.

Any handedness, or kinetic helicity, present in the turbulent flows at the photosphere might also systematically inject "self" magnetic helicity. The dominant source of handedness would presumeably be the coriolis force, which most strongly affects the largest, most slow-moving convective cells. A study of photospheric flow patterns (Hathaway et al. 2000) reveals that supergranules, surface manifestations of large-scale upflows in the subsurface convection, dominate the power spectrum. The supergranular flow pattern is clearly present in the MDI data in figure 2.9, an image of the Sun's magnetic field: the supergranules are the large, circular, field-free areas between concentrations of magnetic flux.

Supergranules' spatial scales are near 20 Mm, and their lifetimes are of the order of a day (Leighton et al., 1962; and see Simon et al., 1988 and references therein). Since the solar rotation period, $\sim$ 24 days, is much longer than the supergranular lifetime, one would not expect the coriolis force to induce much handedness in supergranular flows directly. It is possible that kinetic helicity cascading from very

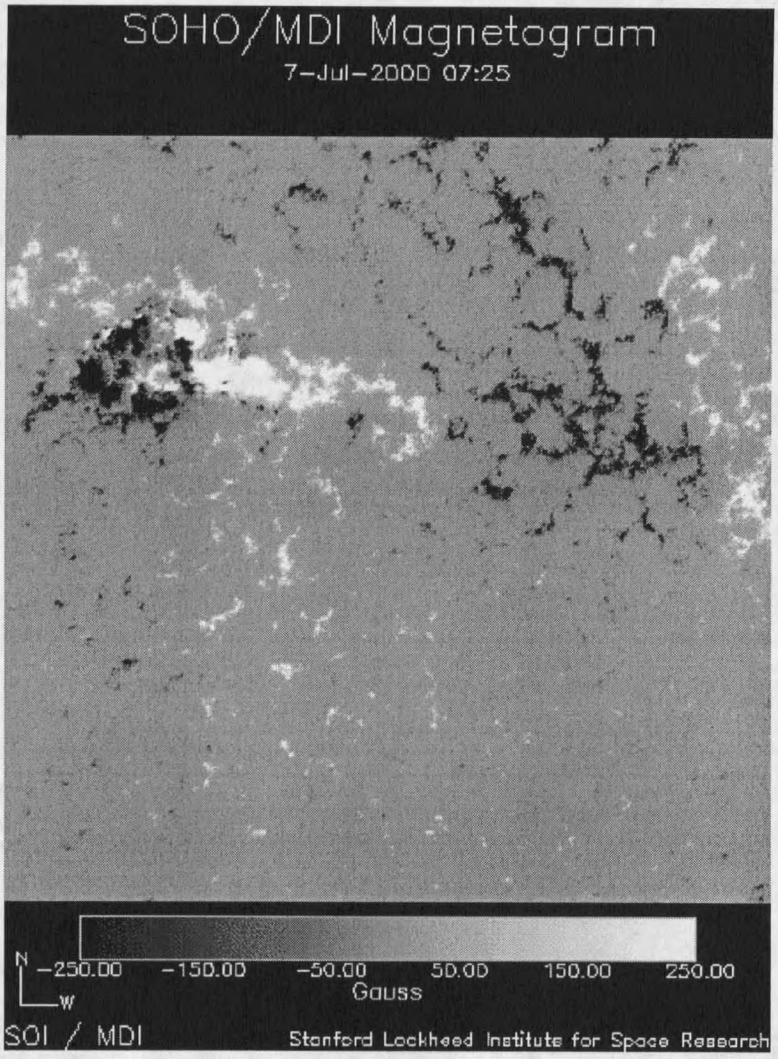

Figure 2.9: Supergranulation Pattern in MDI Data. In this MDI magnetogram, large, circular, field-free supergranules are clearly visible between concentrations of magnetic flux.

large scales, where the coriolis force is relevant, to smaller scales might impart a handedness to smaller scale flows. Crude estimates for the strength of this effect, however, (see Appendix A) imply that such a cascade, even if present, would not have observational consequences.

Whether the coriolis force induces kinetic helicity or not, it is likely that whatever kinetic helicity *is* present in supergranular flows would be concentrated in the observed small-scale downflows at supergranular boundaries, in a manner similar to the concentration of random angular momentum present in bathwater leading to a vortex as a bathtub is drained. Indeed, observations have shown that vorticity in the photospheric flow tends to be concentrated at supergranule boundaries, in regions of converging flow, or downflow (Wang et al. 1995). Since magnetic flux elements tend to cluster in downflow lanes (Simon et al. 1988), this "bathtub effect" might cause winding of individual flux elements, leading to a flux of "self" magnetic helicity from each element.

Since just as much kinetic helicity would be present in the upflows as in the downflows, one might argue against any net effect. But the length scales of the supergranules are greater than the length scales of the downflow lanes, so

$$\omega_{\rm SG} \sim v_{\rm SG}/R_{\rm SG} < \omega_{\rm DL} \sim v_{\rm DL}/R_{\rm DL} \quad , \tag{2.59}$$

where $v_{\rm SG} \sim v_{\rm DL} \sim .5$ km/s, and $L_{\rm SG} \sim 20$Mm $> L_{\rm DL} \sim 10$Mm (Simon et al. 1994). And observations have shown that the power in the vorticity, relative to that in the divergence, is stronger at smaller spatial scales (Wang, 1995, and Tarbell et al., 1994). Hence, the vorticity concentrated in downflows might have a stronger effect on flux elements than that present in upflows.

These ideas are schematically illustrated in figure 2.10, which shows how coriolis-induced vorticity in the northern hemisphere might "wind" magnetic fluxes in downflow regions.

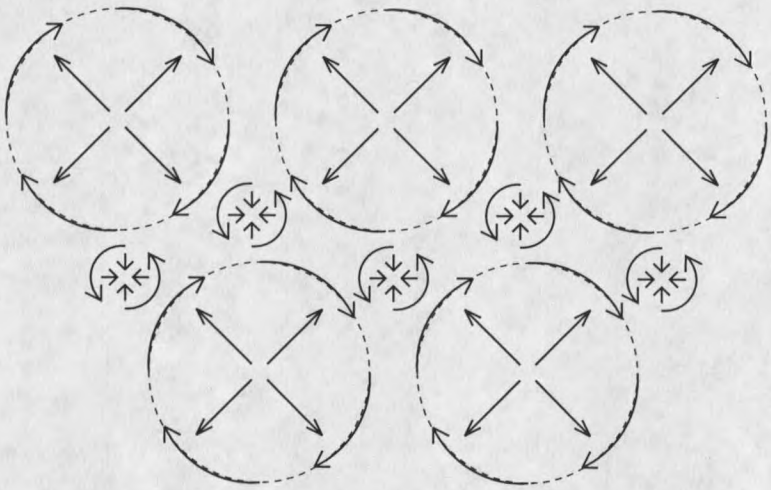

Figure 2.10: Coriolis-Induced Vorticity in Turbulence Spins Fluxes. In this schematic of coriolis-induced vorticities in upflows (within dashed lines delineating supergranules, where the flow diverges) and downflows (between supergranules, where the flow converges) in the Sun's northern hemisphere, flux elements in the downflow regions would be spun by the flow, via a "bathtub effect."

Since self helicity goes as the square of the magnetic flux Φ, and is linear in the angular velocity ω, any bias in the distribution of kinetic helicity, and hence

ω, would lead to a bias in the flux of self helicity. Accordingly, if the coriolis force does impart kinetic helicity of differing signs to the convective turbulence in the northern and southern hemispheres, this might lead to a hemispheric asymmetry in the flux of "self" helicity.

Example: A Rotating Bipole

To illustrate the concepts presented in the previous sections, we use the expressions derived above to quantify the helicity flux in a simple example. For concreteness, we consider two isolated, oppositely-signed fluxes $\Phi_+ > 0$ and $\Phi_- < 0$, separated by a distance $2R$, whose centers of flux are rotating with angular velocity Ω, in a right-hand sense about an axis in the direction of increasing z through the midpoint $\mathcal{O}$ of the line joining their centers of flux. We assume the fluxes' separation, $2R$, is much greater than the diameter $a_\pm$ of either. The geometry of the system is illustrated in figure 2.11.

For purposes of calculating the helicity flux through the photosphere due to the motion of the flux elements, the initial topology of their field lines is irrelevant: they may share flux only with each other, or they may share flux with "infinity" (i.e., other fluxes far from $\mathcal{O}$) or some combination of the two; and the initial fields may or may not have non-zero relative helicity. Accordingly, we leave the topology

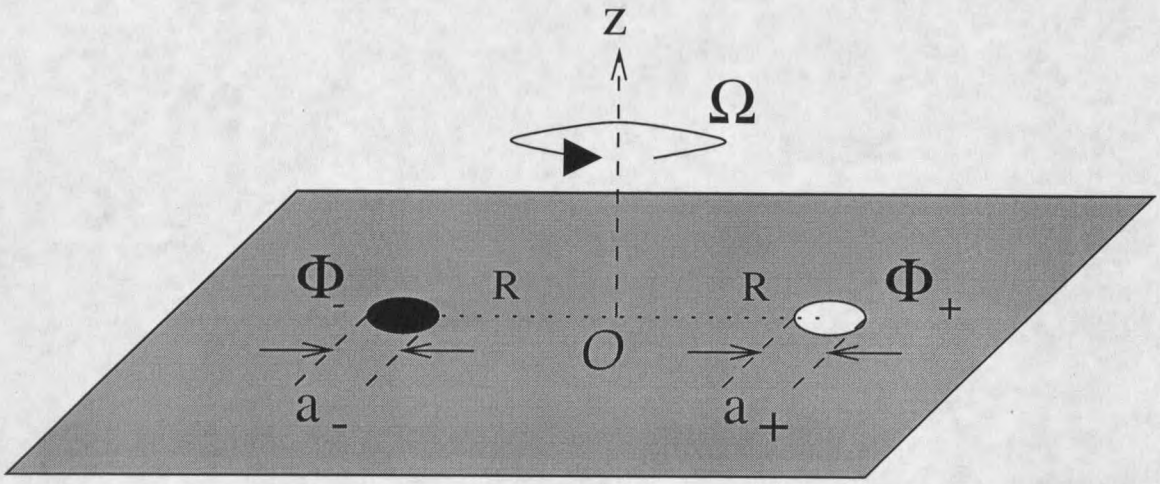

Figure 2.11: Coordinate System in Rotating Bipole Example. Two fluxes, Φ_- (black) and Φ_+ (white), rotate with angular velocity Ω about an axis through $\mathcal{O}$, the midpoint of the line between their centers of flux, a distance $2R$ apart. The fluxes' diameters, $a_\pm$, are much less than their separation. Note that they rotate in a right-hand sense.

and initial helicity unspecified.

We first compute the mutual helicity flux in the system, employing equation (2.16),

$$\frac{d\mathcal{H}^{(\mathrm{MUT})}}{dt} = -\frac{1}{\pi}\sum_i \sum_{j\neq i} \Phi_i \Phi_j \Omega_{ij} \ . \tag{2.60}$$

It turns out that the "relative rate of rotation" of one flux about another is equal to the rate of either flux's rotation about the origin,

$$\Omega = \Omega_{ij} = \Omega_{ji} \ . \tag{2.61}$$

Then the mutual helicity flux is easily calculated to be

$$\frac{d\mathcal{H}^{(\mathrm{MUT})}}{dt} = -\frac{2}{\pi}\Phi_-\Phi_+\Omega \ . \tag{2.62}$$

To compute the self helicity flux from equation (2.56)

$$\frac{dH^{(\mathrm{SELF})}}{dt} = -\frac{\Phi^2}{\pi}\left(C + \left(XF_2^{(1)} - TG_2^{(1)}\right)\right) \ , \tag{2.63}$$

requires specification of the components C, X, and T of the local velocity field in the comoving frame, at each flux's center of flux, and different assumptions about local velocities can lead to different self helicity fluxes.

We can make the assumption that the entire surface rotates rigidly at the angular velocity Ω consistent with the center-of-flux motion. Then the velocity at any point on the surface can be found from

$$\mathrm{v}(r,\phi) = \Omega r(\hat{z} \times \hat{r}) = \Omega r\hat{\phi} \ , \tag{2.64}$$

where (r, ϕ, z) are the usual cylindrical coordinates, centered at $\mathcal{O}$. In this case, the X and T components of the flow vanish, and we only need to consider the

contribution from the C term, which we compute to be

$$\begin{aligned} C &= \omega_z && (2.65)\\ &= \frac{1}{2}(\nabla \times \mathbf{v})_z && (2.66)\\ &= \frac{1}{2}\left(\frac{1}{r}\frac{\partial(rv_\phi)}{\partial r} - \frac{1}{r}\frac{\partial v_r}{\partial \phi}\right) && (2.67)\\ &= \Omega \ . && (2.68) \end{aligned}$$

(This is analogous to the rotation of the Moon about its axis once – with respect to the Earth – for every orbit it completes around the Earth.) We then find the self helicity flux to be

$$\frac{dH^{(\mathrm{SELF})}}{dt} = -\frac{1}{\pi}\Phi_-^2\Omega - \frac{1}{\pi}\Phi_+^2\Omega \ . \tag{2.69}$$

Computing the total helicity flux, we have

$$\begin{aligned} \frac{dH^{(\mathrm{TOT})}}{dt} &= \frac{dH^{(\mathrm{MUT})}}{dt} + \frac{dH^{(\mathrm{SELF})}}{dt} && (2.70)\\ &= -\frac{2}{\pi}\Phi_-\Phi_+\Omega - \frac{1}{\pi}\Phi_-^2\Omega - \frac{1}{\pi}\Phi_+^2\Omega && (2.71)\\ &= -\frac{1}{\pi}\Omega(\Phi_- + \Phi_+)^2 \ . && (2.72) \end{aligned}$$

If $|\Phi_-| \neq \Phi_+$, then there is a net helicity flux: the flux imbalance implies that a monopole moment exists, and rotating the footpoints of field lines which extend

to infinity must lead to a net winding of field lines and, hence, a helicity flux.

If, however, we assume $|\Phi_-| = \Phi_+ = \Phi_0$, then the total helicity flux vanishes. If Φ_- and Φ_+ only share flux with each other, then, viewed qualitatively, this result makes sense: the entire corona rotates rigidly, and no field lines wind around each other; hence there is no flux of helicity. (If field lines run from Φ_- and Φ_+ to other fluxes, then there is winding of field lines, but no *net* winding.)

If we alter our "rigid rotation" assumption for the velocity on the surface, and assume instead that, as each flux orbits $\mathcal{O}$, it keeps a *constant orientation* with respect to a fixed frame of reference, then the self helicity flux vanishes. So the total helicity is just the mutual helicity flux,

$$\frac{dH^{(\mathrm{TOT})}}{dt} = \frac{dH^{(\mathrm{MUT})}}{dt} + 0 \tag{2.73}$$

$$= -\frac{2}{\pi}\Phi_-\Phi_+\Omega \tag{2.74}$$

$$\neq 0 \ . \tag{2.75}$$

Figure 2.12 illustrates the difference in the fluxes' orientations between the "rigid rotation" and "constant orientation" cases: the fluxes also rotate about their own centers of flux in the former (left), while they do not in the latter (right).

We also note that, in the "constant orientation" case, if $\Phi_- = -\Phi_+$, and the fluxes are only linked to each other, then this "mutual helicity flux" arises from

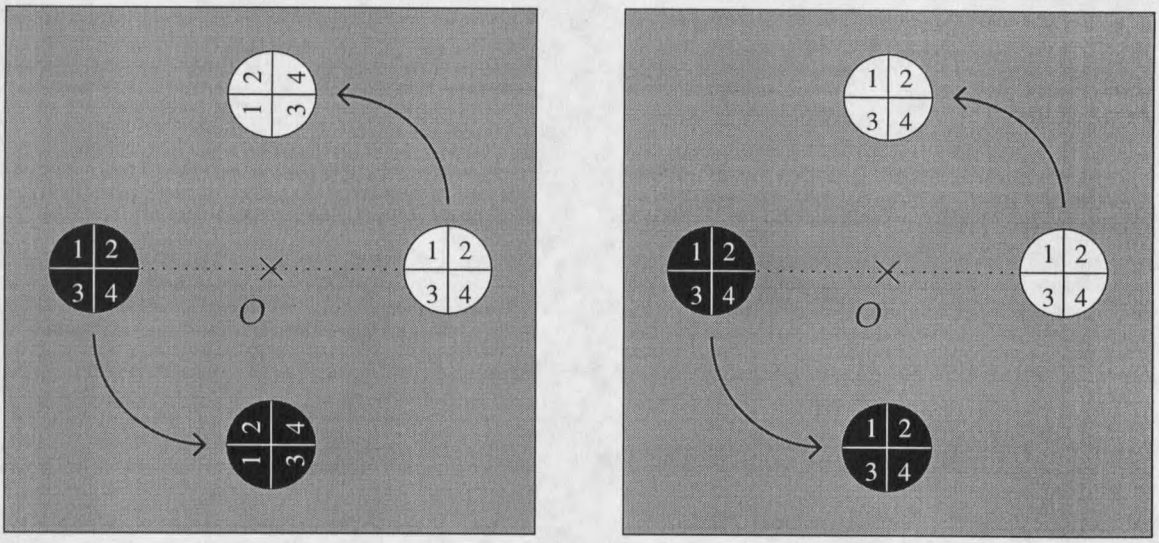

Figure 2.12: "Rigid Rotation" and "Constant Orientation" Assumptions. Fluxes "orbit" ($\pi/2$) radians about $\mathcal{O}$ under differing assumptions about each flux's orientation as it orbits. If one assumes the entire surface undergoes a rigid rotation, then each also rotates about its center of flux (left). One can assume instead that each flux keeps a constant orientation, in which case each does *not* rotate about its axis (right).

the winding of field lines entirely within the topological domain linking Φ_- and Φ_+. The resultant state, therefore, would possess a non-zero "self" helicity. In this case, the division of the total helicity *flux* into mutual/self components does not correspond to the division of the total *helicity* into mutual/self helicities. If we were to calculate the helicity flux in the corotating frame, however, then the mutual helicity flux would vanish, the self helicity flux would be non-zero (since each flux would appear to be rotating about its axis), and the division of helicity flux would match the division of the helicity itself.

Evidently, the division of the helicity flux into mutual/self contributions is not unambiguous. In fact, the ambiguity is more than an artifact of the frame of reference used in the calculation: the mutual/self division of the *helicity* depends upon the field's topology, which is *not* determined by the distribution of fluxes on the boundary surface, while the mutual/self division of the helicity flux *only* depends on the distribution of fluxes on the boundary.

CHAPTER 3

METHODS

Data

To determine the rate of helicity flux using the methods outlined in the previous chapter, we have to track both the positions of magnetic flux elements and their structural attributes.

We have analyzed line-of-sight magnetograms taken with the Michelson Doppler Imager (MDI) onboard the Solar and Heliospheric Observatory (SoHO) for the photospheric magnetic field B_z used in our study. This instrument finds the magnetic field by inverting the Stokes V profile in the Ni I (6768 Å) line, which is formed at the photosphere. There is some indication that the inversion approach is subject to systematic errors at very high or very low field strengths: apparently, both are underestimated (Dr. Alex Pevtsov, private communication). An analysis of this issue is beyond the scope of this work; we simply take the magnetic field strengths returned by the instrument team without analyzing possible systematic errors in their results.

The data analyzed were all taken in the instrument's "high resolution" mode, with .61" pixels. At SoHO's position at the L1 point between the Earth and the Sun, this corresponds to about 442 km on the Sun. A full image contains 1024×1024 pixels; the "hi-res" field of view (FOV) is illustrated in figure 3.1. Roughly, it is centered at 10° (in heliocentric degrees) north of the Sun's equator, at the central meridian of the disk, and is about 37° (in heliocentric degrees) on a side. Precise pointing information is returned with each image.

We tracked fluxes in five sequences for 7.5 hours or longer, in regions of predominantly quiet sun near solar minimum. Three tracking sequences were from the same observing campaign; we label each sequence as a subset of data set #2. Data sets #1 and #3 were tracked by Hagenaar et al. (1999), which allows comparison between some of our results and theirs. The observing times, durations, and pointings of the tracking runs are listed in table 3.1.

To improve the signal-to-noise ratio in our data, we average five "good" magnetograms, usually with 1 minute cadence. Occasionally, however, missing or "bad" magnetograms increase the time between averaged images. We define a "bad" magnetogram as one in which more than 1000 pixels are either labelled blank, or exceed 800 G in absolute value; these are simply skipped over in finding five magnetograms to average. To give some idea of the frequency with which bad magnetograms are found, we note that only 8 occurred in the 15+ hours of data

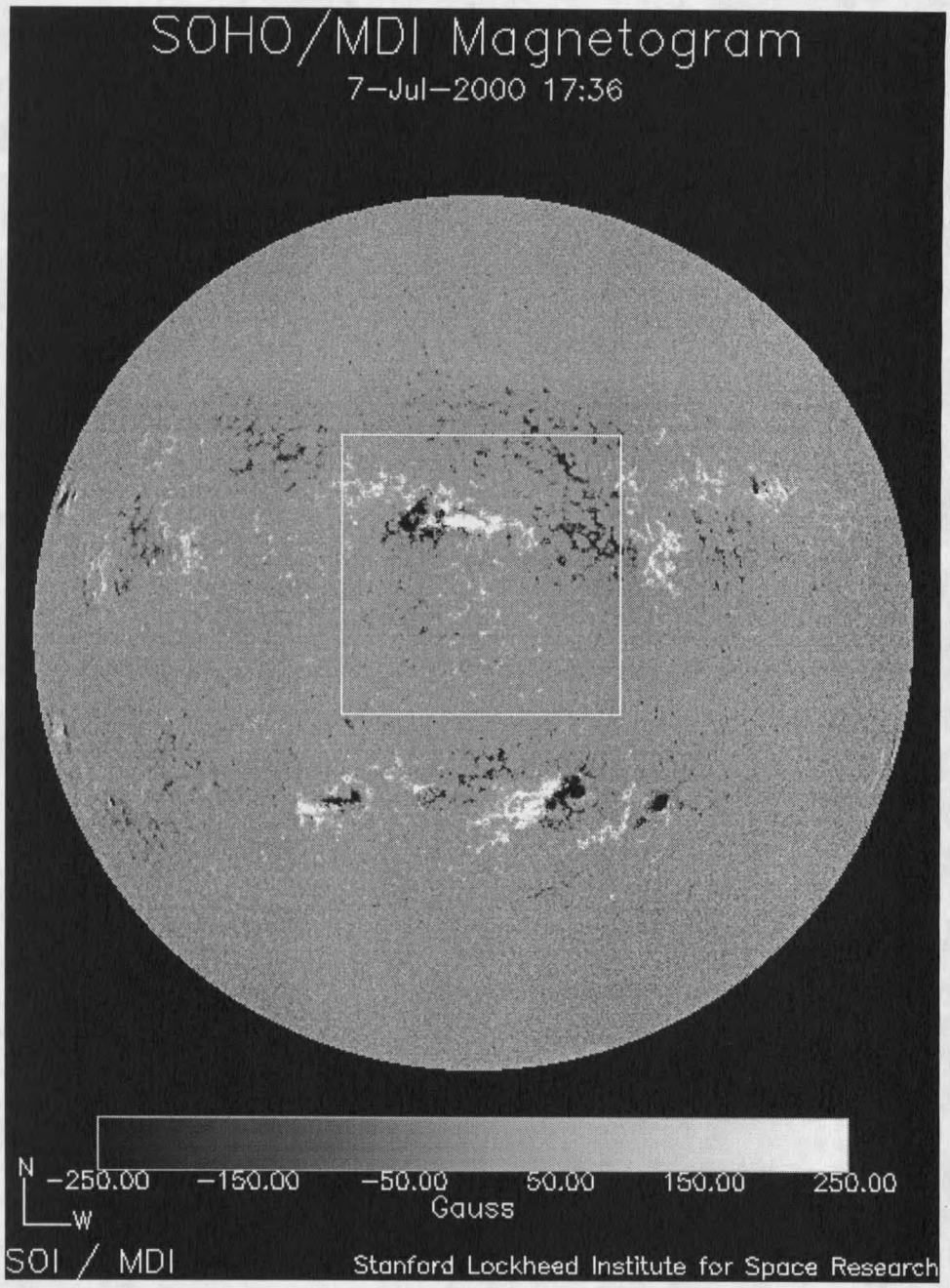

Figure 3.1: MDI Hi-Res FOV. The high resolution, or "hi res," field of view (FOV) of the MDI instrument is centered about 10° (in heliocentric degrees) north of the Sun's equator, near the central meridian of the disk, and is about 37° (in heliocentric degrees) on a side.

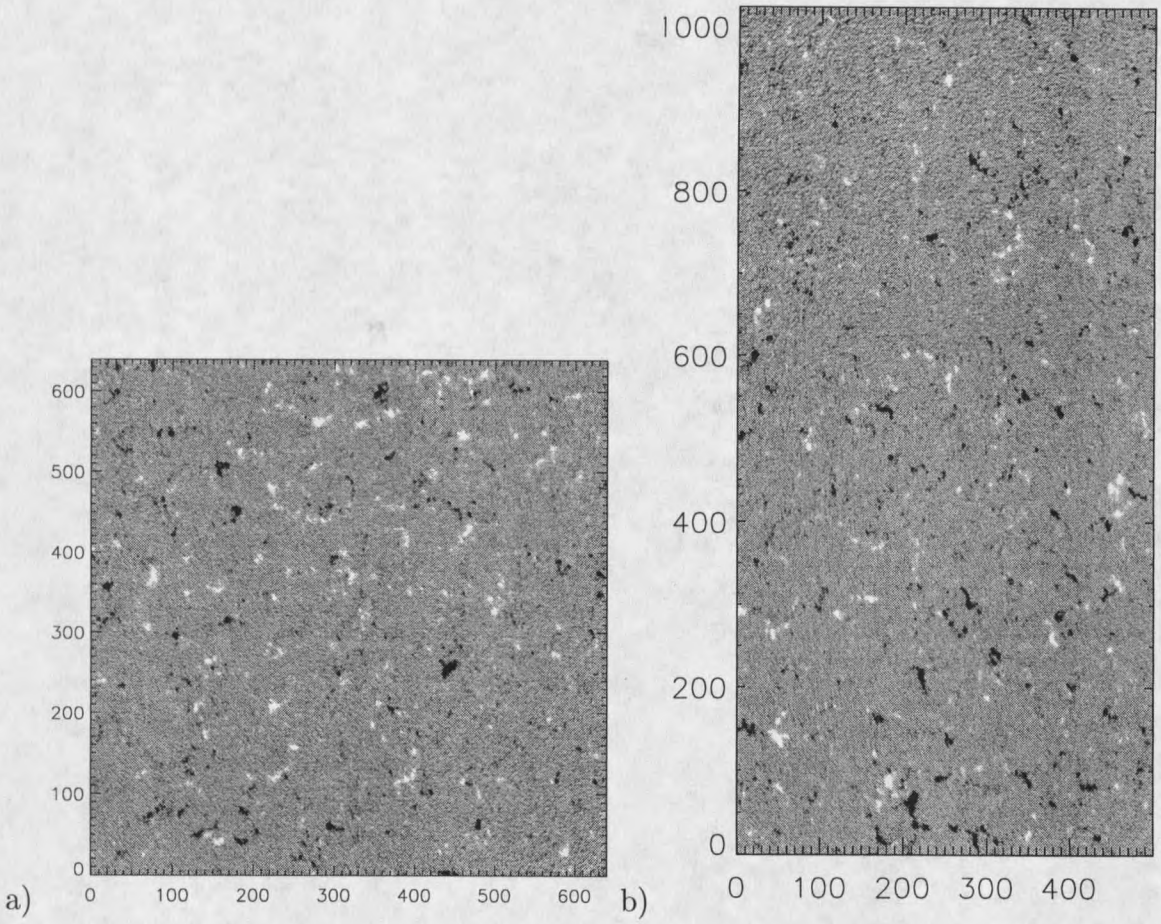

Figure 3.2: Images from Data Sets # 1 and 2a. The first contrast-enhanced, unsmoothed, five-magnetogram average images from data sets # 1 (left) and 2a (right). A small active region to the left (east) of the FOV in data set # 1 was cropped from the full image.